

Article

Spatiotemporal Variations in Reference Evapotranspiration and Its Contributing Climatic Variables at Various Spatial Scales across China for 1984–2019

Xiaohui Yan ^{1,*} , Abdolmajid Mohammadian ² , Ruigui Ao ¹, Jianwei Liu ¹ and Xin Chen ²

¹ School of Water Resources Engineering, Dalian University of Technology, 2 Ling Gong Road, Dalian 116024, China

² Department of Civil Engineering, University of Ottawa, 161 Louis Pasteur, Ottawa, ON K1N 6N5, Canada

* Correspondence: yanxh@dlut.edu.cn

Abstract: Reference evapotranspiration (ET_0) is of great significance in studies of hydrological cycle, agricultural water resources, and hydrometeorology. The present study collected daily meteorological data at 536 meteorological stations in China from 1984 to 2019, calculated daily ET_0 using the FAO Penman–Monteith equation, analyzed the spatial distribution and temporal variation characteristics of ET_0 and meteorological variables at four different spatial scales (continental, regional, provincial, and local), and discussed the sensitivity of ET_0 to the meteorological variables and the contribution rates of the meteorological variables to the ET_0 variations. The results showed that ET_0 increased at 406 out of the 536 stations (75.7%), with the trends being significant at 65 stations at the 5% significance level, and 147 at the 1% significance level. The slope calculated using Sen's method and linear trend method showed that the annual ET_0 at the continental scale increased by approximately 12 mm/decade. Most of the stations showed decreasing trends in relative humidity (H_m), sunshine duration (S_D), and wind speed at 2 m height (U_2) while increasing trends in the maximum air temperature (T_{max}) and minimum air temperature (T_{min}). ET_0 was most sensitive to H_m (sensitivity coefficient, $S_t = -0.66$), followed by T_{max} ($S_t = 0.29$), S_D ($S_t = 0.18$), U_2 ($S_t = 0.16$), and T_{min} ($S_t = 0.07$). Most of the stations showed increasing trends in S_t for H_m (56.16%), T_{max} (72.95%), T_{min} (87.31%), and U_2 (90.49%), and decreasing trends for S_D (69.78%). The variations in H_m , T_{max} , and T_{min} increased the ET_0 at most of the stations (82.28%, 98.13%, and 69.03%, respectively). The variations in S_D and U_2 decreased ET_0 at most of the stations (66.04% and 56.34%, respectively). Some ET_0 characteristics in a few regions can be well described using a single spatial scale. However, most regions exhibited significantly different ET_0 characteristics across spatial scales. The results of this project can provide reference for hydrological analysis and agricultural water management under climate change conditions and provide data and information for other hydrology-related applications.

Keywords: reference evapotranspiration; spatial scale; climatic variables; trend analysis; sensitivity analysis; contribution analysis



Citation: Yan, X.; Mohammadian, A.; Ao, R.; Liu, J.; Chen, X.

Spatiotemporal Variations in Reference Evapotranspiration and Its Contributing Climatic Variables at Various Spatial Scales across China for 1984–2019. *Water* **2022**, *14*, 2502. <https://doi.org/10.3390/w14162502>

Academic Editor: Maria Mimikou

Received: 19 June 2022

Accepted: 11 August 2022

Published: 14 August 2022

Publisher's Note: MDPI stays neutral with regard to jurisdictional claims in published maps and institutional affiliations.



Copyright: © 2022 by the authors. Licensee MDPI, Basel, Switzerland. This article is an open access article distributed under the terms and conditions of the Creative Commons Attribution (CC BY) license (<https://creativecommons.org/licenses/by/4.0/>).

1. Introduction

Evapotranspiration (ET) is known as a key parameter reflecting the variations in the climate and is a major component of the meteorological and hydrological cycles [1–9]. With the risk of heatwave events and their persistence intensifying in recent past and increasing faster, the ET, precipitation, and other climatic variables have changed over the diverse regions [10,11]. In many hydrodynamic and water quality modeling system, the ET can be directly used as an input variable, so it is important to better understand the spatiotemporal features of ET and the contributing factors in the context of ongoing climate change. Furthermore, a better understanding of ET is beneficial for analyzing the hydrodynamics and water quality, especially in terms of explaining the mechanisms for the variations in water quality, such as the variations in the balance of salinity and variations in contaminant

concentrations. ET can be estimated by the reference evapotranspiration (ET_0). It has been widely accepted that ET_0 is an important factor in water balance and conversion and is thus its estimation and forecasting is important in water resources management [12–17]. For example, estimating crop water demand is a necessary step in irrigation scheduling and the design of agricultural water conservancy projects, and the estimation of crop water demand is mainly based on the calculation of ET_0 [18,19]. A clear understanding of the spatiotemporal variations in ET_0 is of importance for better planning and management of water resources. Contrary to intuitive expectation, ET_0 has been reported to decrease in many regions with increasing temperature [20–22], and this controversial behavior is known as the “evaporation paradox” [23–25]. The “evaporation paradox” actually provides a straightforward indication that the ET_0 variations are products of changes in multiple variables rather than any one variable, and it has attracted many researchers to investigate the spatiotemporal variations in ET_0 and its contributing climatic factors.

Tang et al. [18] investigated ET_0 and its contributing meteorological variables in the Haihe River Basin of northern China and found that ET_0 exhibited a decreasing trend with a rate of -1 mm yr^{-2} ; the air temperature produced an increase in the derivative of ET over time (dET_0/dt), while the net radiation and wind speed produced a decrease in (dET_0/dt). Liu and McVicar [24] studied the potential evaporation and its contributing climatic factors in the Yellow River Basin in China and found that the potential evaporation in the water yielding region showed an increasing trend, while that in the water consuming region exhibited a decreasing trend during 1961–2010. Fully physics-based models should be employed to explicitly describe the contributing effects of the climatic factors on potential evaporation. Wang et al. [26] studied the spatial and temporal variations in ET_0 and the meteorological variables in China for the period 1961–2013 using a $0.5^\circ \times 0.5^\circ$ gridded dataset; the study showed that there was a significant spatiotemporal variability in ET_0 , and the overall annual ET_0 declined at a rate of 6.84 mm/decade. The variation in ET_0 was mostly attributed to the wind speed (U_w), followed by the maximum air temperature (T_{\max}), sunshine duration (S_D), relative humidity (H_m), and minimum air temperature (T_{\min}). Jiang et al. [27] found that during the growing season in Southwest China ET_0 decreased at a rate of 10.25 mm/decade for the period 1961–1996 and increased at a rate of 8.12 mm/decade for the period 1997–2016; ET_0 was most sensitive to H_m , followed by S_D , T_{\max} , T_{\min} , and U_w . Yan et al. [7] investigated the importance of the meteorological variables in predicting ET_0 at eight stations in China; the results indicated that the ET_0 in the arid region was mostly influenced by U_w , followed by S_D and H_m , and ET_0 in the humid region was mostly influenced by S_D , followed by H_m and U_w .

Although the existing studies have provided valuable understanding of the spatial and temporal variability in ET_0 and the relevant meteorological variables in China, a major drawback of all these works is that they have only examined the characteristics at a single or two spatial scales [28–31]. The resulting findings of these previous studies cannot provide sufficient information for some large water conservancy projects that need to consider both global and local factors, and it is still unclear whether the global values derived from the data at discrete observation points can satisfactorily represent the local characteristics due to the lack of comparisons between observations across spatial scales.

Therefore, in contrast to the existing studies of ET_0 in China, there is a lack of comprehensive datasets of ET_0 distribution at different spatial scales across China. The primary purpose of the present study was to investigate the variability in ET_0 and its contributing climatic variables at various spatial scales. A total of four different spatial scales were considered, including continental, regional, provincial, and local. To specify, the present study was conducted toward achieving the following objectives: (1) to provide a new dataset of daily ET_0 at different spatial scales in China for 1984–2019, calculated using the FAO Penman–Monteith equation; this comprehensive dataset and the resulting findings do not currently exist in the literature and are important for projects that require both global and local considerations; (2) to analyze the spatial distribution and temporal variation characteristics of ET_0 and meteorological variables at different spatial scales adopting the

non-parametric Mann-Kendall test method; and (3) to quantitatively analyze the sensitivity of ET_0 to the meteorological variables and the contribution rates of the meteorological variables to ET_0 variations using the partial derivative sensitivity coefficients method, and determine the key climatic variables affecting ET_0 at different spatial scales.

2. Materials and Methods

2.1. Study Area and Climate Dataset

Located in the east of Asia, China is the third largest country in the world in land area, with an estimated land area of 9.6 million square kilometers and a population of over 1.4 billion. Its terrain is generally high in the West and low in the East. Most of the areas belong to temperate and subtropical monsoon climate, with rich and diverse climate types and geographical landscape. The issues surrounding in China are severe partially because it has uneven spatial and temporal distribution of water resources. The precipitation generally decreases from the southeast coast to northwest inland. The cultivated land in the Yangtze River Basin and south of the Yangtze River only accounts for 36% of China's total, while water resources account for 80% of China's total. In the Yellow River, Huaihe River and Haihe River basins, water resources only account for 8% of China's total, while arable land accounts for 40% of China's total. The annual and interannual variation of precipitation and runoff is large. These characteristics of water resources cause frequent floods and droughts in China, and agricultural production is also relatively unstable.

In the present study, a total of four spatial scales were considered: continental, regional, provincial, and local. The continental scale was equivalent to the national scale, which covered mainland China. At the regional scale, the study area has been divided into 7 sub-regions by the following geographic locations: North Eastern Region (NER), North China Region (NCR), East China Region (ECR), South China Region (SCR), Central China Region (CCR), North Western Region (NWR), and South Western Region (SWR). A large portion of the water resources activities in China are governed by provincial water management authorities, so the provincial scale was also considered. The local scale considered the stations that have sufficient quality data.

The daily climatic data employed in this study included daily H_m , S_D , T_{max} , T_{min} , and U_w at 10 m height (U_{10}). The data of U_{10} has been converted to U_2 (U_w at 2 m height) using the transformation formula provided by Allen et al. [32]. The data were primarily obtained from the China Meteorological Administration. The quality of the dataset has been carefully controlled, and the dataset has been widely used in previous studies [9,24,28]. There were 665 stations in the original dataset, but 129 of the stations were excluded because they had extensive missing data; finally, 536 stations were selected. The study area and selected meteorological stations are presented in Figure 1. The subregions, the provinces, and the corresponding numbers of meteorological stations are provided in Table 1.

Table 1. The study area, province, and corresponding number of stations.

Sub-Region	Province and Number of Stations
NCR	BeiJing (BJ; 2), HeBei (HB; 18), NeiMenggu (NM; 26), TianJin (TJ; 2), ShanXi (SX; 18)
NER	HeiLongjiang (HL; 30), JiLin (JL; 17), LiaoNing (LN; 21)
ECR	ShangHai (SH; 1), AnHui (AH; 6), FuJian (FJ; 17), JiangSu (JS; 10), JiangXi (JX; 16), ShanDong (SD; 19), ZheJiang (ZJ; 15)
SCR	GuangDong (GD; 36), GuangXi (GX; 18), HaiNan (HI; 5)
CCR	HeNan (HA; 15), HuBei (HB; 16), HuNan (BN; 22)
NWR	GanSu (GS; 23), NingXia (NX; 10), QingHai (QH; 25), ShanXi (SX; 17), XinJiang (XJ; 33)
SWR	GuiZhou (GZ; 17), SiChuan (SC; 35), XiZang (XZ; 17), YunNan (YN; 25), ChongQing (CQ; 4)



Figure 1. The study area and locations of the meteorological stations (the dots).

2.2. ET_0 Calculation

The present study employed the FAO Penman–Monteith (P–M) equation to calculate the daily ET_0 . In March 1990, the Food and Agriculture Organization of the United Nations (FAO) recommended the use of this formula to calculate ET_0 at the international symposium on crop evapotranspiration calculation methods held in Rome, Italy [19]. The formula is the most widely used method to calculate ET_0 in the world. The P–M formula, physically based on both the energy balance and aerodynamics, does not need a special regional calibration function, and it can calculate ET_0 by using general meteorological data, which has high practical value and accuracy [33]. The equation can be written as

$$ET_0 = \frac{0.408\Delta(R_n - G) + \gamma[900/(T + 273)]U_2(e_s - e_a)}{\Delta + \gamma(1 + 0.34U_2)} \quad (1)$$

where ET_0 is the reference evapotranspiration (mm day^{-1}); Δ is the slope vapor pressure curve ($\text{kPa } ^\circ\text{C}^{-1}$); R_n is the net radiation at the crop surface ($\text{MJ m}^{-2} \text{day}^{-1}$); G is the soil heat flux density ($\text{MJ m}^{-2} \text{day}^{-1}$); γ is the psychrometric constant ($\text{kPa } ^\circ\text{C}^{-1}$); T is the mean daily air temperature at 2 m height ($^\circ\text{C}$); U_2 is the U_w at the 2m height (m/s); e_s is the saturation vapor pressure (kPa); e_a is the actual vapor pressure (kPa). The intermediate variables can be calculated from daily H_m , S_D , T_{\max} , T_{\min} , and U_2 , following the equations provided in the FAO56 report [32].

2.3. Trend Analysis

The present study used the Mann–Kendall trend test approach to detect significant trends in ET_0 and its contributing climatic variables. The Mann–Kendall (MK) test [34–36] is a nonparametric (distribution-free) test, and it was employed in this study because it has been widely used in assessing whether there is a monotonic upward or downward trend of hydrological variables over time [27,37]. Its superiority exists in the ability of detecting the significance of the long time-series trend, no matter the sample series follow a certain type

of distribution [38]. In the MK test, S is a statistical value used to determine whether values obtained later in time tend to be larger than values obtained earlier, as:

$$S = \sum_{i=2}^n \sum_{j=1}^{i-1} \text{sign}(x_i - x_j), \quad (2)$$

where n is the number of observations and $\text{sign}(x_i - x_j)$ can be expressed as:

$$\text{sign}(x_i - x_j) = \begin{cases} -1 & \text{if } (x_i - x_j) < 0 \\ 0 & \text{if } (x_i - x_j) = 0 \\ 1 & \text{if } (x_i - x_j) > 0 \end{cases}, \quad (3)$$

The variance of S can be computed as follows:

$$\text{Var}(S) = \frac{n(n-1)(2n+5) - \sum_{k=1}^l t_k(t_k-1)(2t_k+5)}{18}, \quad (4)$$

where l is the number of tied groups, and t_k is the number of observations in the t th group.

The MK test statistic, Z_S , can be expressed as:

$$Z_S = \begin{cases} \frac{S+1}{\sqrt{\text{Var}(S)}} & \text{if } S < 0 \\ 0 & \text{if } S = 0 \\ \frac{S-1}{\sqrt{\text{Var}(S)}} & \text{if } S > 0 \end{cases}, \quad (5)$$

Positive values of Z_S indicate that the variables of interest tend to increase with time, and negative values of Z_S indicate that the variables of interest tend to decrease with time. The null hypothesis of no trend is rejected when $|Z_S| > 1.96$ at the $\alpha = 0.05$ level and $|Z_S| > 2.576$ at the $\alpha = 0.01$ level.

To estimate the slope of the linear trend, the time series of a variable (e.g., ET_0) were fitted into a linear regression equation, such as

$$ET_0 = T_L \cdot t + b \quad (6)$$

where T_L is slope of the linear trend.

The slope of trend can also be estimated using a nonparametric procedure developed by Sen [39]. In the procedures, the slopes of N pairs of observations are first estimated by

$$Q_i = \frac{x_j - x_k}{j - k} \text{ for } i = 1, \dots, N \quad (7)$$

where x_j is the value at time j , while x_k is the value at time k ($j > k$). Since there is only one datum in each time period in the present study, N can be computed as $N = \frac{n(n-1)}{2}$ and n is the number of time steps. The values of these slopes are then ranked from smallest to largest, and the median value is known as the Sen's estimator of slope. When N is odd, Sen's estimator of slope is $Q_{(N+1)/2}$; when N is even, Sen's estimator of slope is $\frac{Q_{N/2} + Q_{(N+2)/2}}{2}$.

To verify whether the median slope is statistically different from zero, the confidence interval for Sen's estimator of slope, for a given level of significance α , should be computed [34]. The confidence interval can be computed as follows:

$$C_\alpha = Z_{1-\alpha/2} \sqrt{\text{Var}(S)} \quad (8)$$

where $\text{Var}(S)$ is computed by (4), and $Z_{1-\alpha/2}$ is obtained from the standard normal distribution table. The approximate normal theoretical lower and upper confidence limit

are respectively the M_1 th largest and the (M_2+1) th largest of value of Q . M_1 and M_2 are defined by

$$M_1 = \frac{N - C_\alpha}{2}; M_2 = \frac{N + C_\alpha}{2} \quad (9)$$

the Sen's estimator of slope is statistically different from zero if the two limits $Q(M_1)$ and $Q(M_2)$ have the same sign.

2.4. Sensitivity Coefficient and Contribution Rate

The sensitivity coefficient, St_i , that quantifies the sensitivity of ET_0 to a climatic variable, c_i , can be expressed as [27]:

$$St_i = \frac{\partial ET_0}{\partial c_i} \cdot \frac{c_i}{ET_0} \quad (10)$$

If $St_i > 0$, ET_0 and c_i will increase or decrease simultaneously, otherwise, they have a reverse relation. The larger the $|St_i|$, the greater the effect of a climatic variable has on ET_0 variation. The sensitivity coefficient method is more convenient and accurate compared to other sensitivity analysis approaches [40], and it has been widely used in hydro-meteorological study.

The contribution rate of c_i , C_{bi} , to ET_0 variation, can be expressed as [27]:

$$C_{bi} = St_i \frac{n \times Td_i}{|Ac_i|} \times 100\% \quad (11)$$

where n is the number of observations, Td_i is the trend of the variable c_i , and $|Ac_i|$ is the absolute value of the averaged c_i . If the C_{bi} is positive (negative), it denotes the variable had a positive (negative) contribution to ET_0 variation. The method can clearly reveal how the climatic variables contribute to ET_0 .

3. Results

3.1. Spatiotemporal Variation of ET_0

Figure 2 shows the descriptive statistics of daily ET_0 at the 536 stations. The spatial distribution plots, which were obtained by interpolating the results using the Kriging interpolation approach, are provided primarily for the purpose of visualization. The mean daily ET_0 ranged from around 1 mm (mainly in the northeast) to around 4 mm (such as in the southern edge). The minimum daily ET_0 in the northern part was close to 0 mm, partially because the winter temperature in the north was quite low. The minimum daily ET_0 in the southern part was around 1 mm. Although the temperature increased from north to south, the maximum daily ET_0 showed a reverse trend, which may partially be attributed to the higher U_2 in the northern part, and revealed that ET_0 is the combined result of various climatic variables. The median values were close to the mean values. Generally, the standard deviation and variance decreased from north to south, and the kurtosis and skewness increased from northeast to southwest.

The results of the M-K trend analysis are shown in Figure 3. ET_0 increased at 406 of the 536 stations (75.7%), with the trends being significant at 65 stations at the 5% significance level, and 147 at the 1% significance level. ET_0 decreased at 128 out of the 536 stations (23.9%), with the trends being significant at 13 stations at the 5% significance level, and 13 at the 1% significance level. In general, most of the stations exhibited an increasing ET_0 , and the stations showing significant increasing trends were primarily located in NM, NX, GS, SC, CQ, and YN. The averaged slope calculated using Sen's method and linear trend method were 0.0033 and 0.0034, respectively. Therefore, the annual ET_0 at the continental scale increased by approximately 12 mm/decade in China.

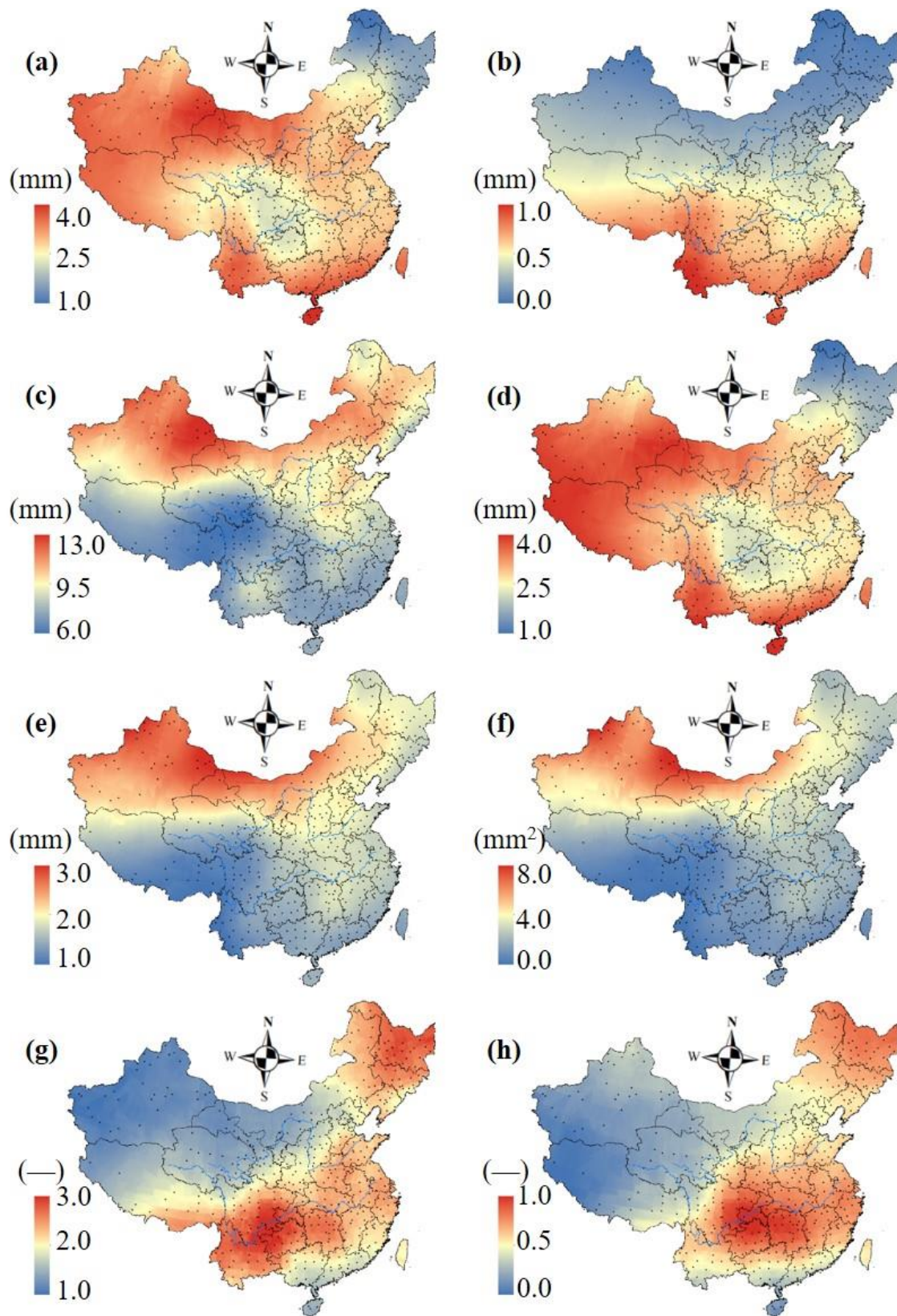


Figure 2. Descriptive statistics of daily ET_0 : (a) mean; (b) minimum; (c) maximum; (d) median; (e) standard deviation; (f) variance; (g) kurtosis; and (h) skewness.

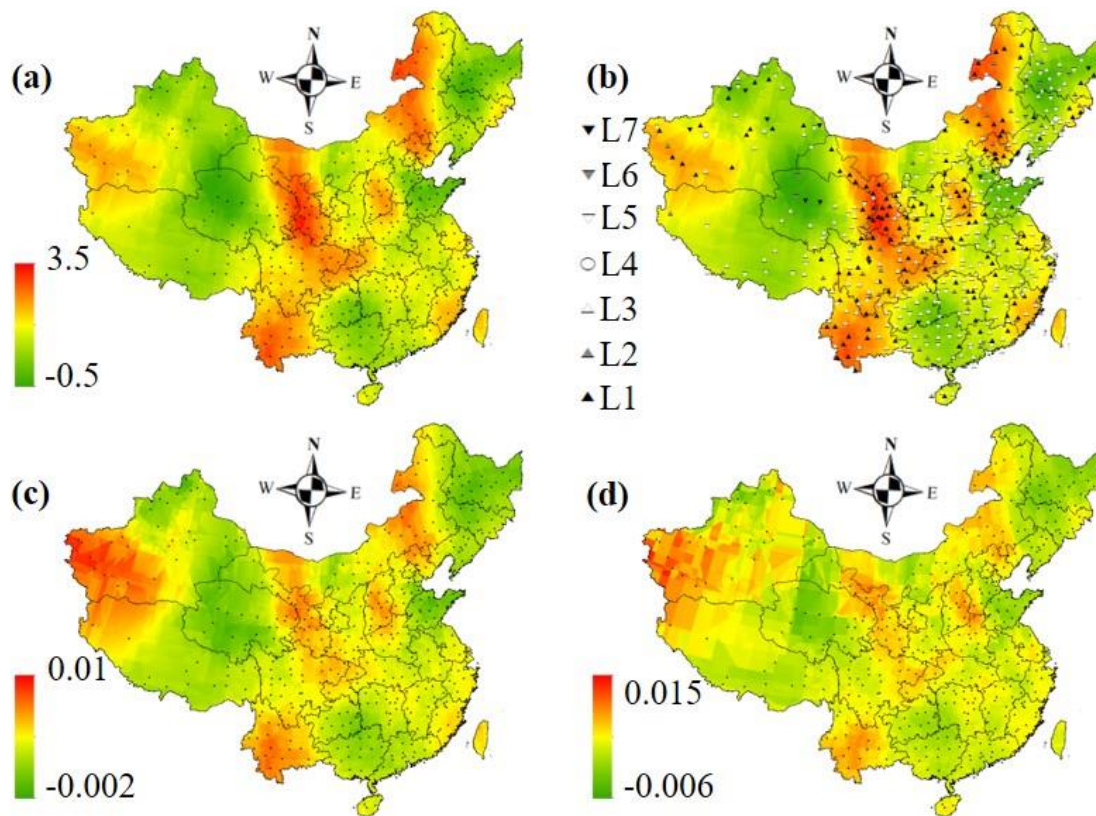


Figure 3. Spatial distribution maps for the trend analysis of ET_0 : (a) M-K Z_5 , (b) significance, (c) Sen's slope, and (d) linear trend. L1: significant-increase (1%); L2: significant-increase (5%); L3: increase; L4: no trend; L5: decrease; L6: significant-decrease (5%); L7: significant-decrease (1%).

3.2. Spatiotemporal Variation of Climatic Factors

The descriptive statistics of the climatic variables were shown in Figure 4. Based on the mean data, H_m increased from the northwest (less than 40%) to the southeast (more than 80%); S_D decreased from west (as high as 9 h) to east (as low as 3 h); T_{max} increased from north (lower than 5 °C) to south (close to 30 °C); T_{min} also increased from north (lower than −10 °C) to south (higher than 20 °C); and U_2 decreased from north (close to 4 m/s) to south (as low as 1 m/s). The median values were close to the mean values. The standard deviations ranged from around 19% in the northwest to around 8% in southeast. Conversely, the standard deviations for S_D increased from the northwest (approximately 4.5 h) to the southeast (approximately 2.5 h). The standard deviations for T_{max} , T_{min} , and U_2 all decreased from north to east. These standard deviations can quantify how accurate it was to estimate climatic variables at a smaller spatial scale using characteristics at a larger spatial scale.

Figure 5 shows the results of trend analysis for the climatic variables. H_m decreased at 443 of the 536 stations (82.6%), and the averaged slopes calculated using Sen's method and linear trend method were −0.089 and −0.086, respectively. The majority of the stations (67.2%) exhibited decreasing S_D , with an average trend slope of −0.006 (Sen's = −0.006; and linear = −0.006). Most of the stations showed increasing T_{max} (532 stations; 99.3%), and the averaged slope was 0.039 (Sen's = 0.040; and linear = 0.039). Similarly, most of the stations (512 stations; 95.5%) had an increasing T_{min} with the averaged slope being 0.042 (Sen's = 0.042; and linear = 0.042). The U_2 showed an overall decreasing trend, as 324 stations (60.4%) had a declining U_2 , and the averaged Sen's slope and linear slope were −0.007 and −0.005, respectively.

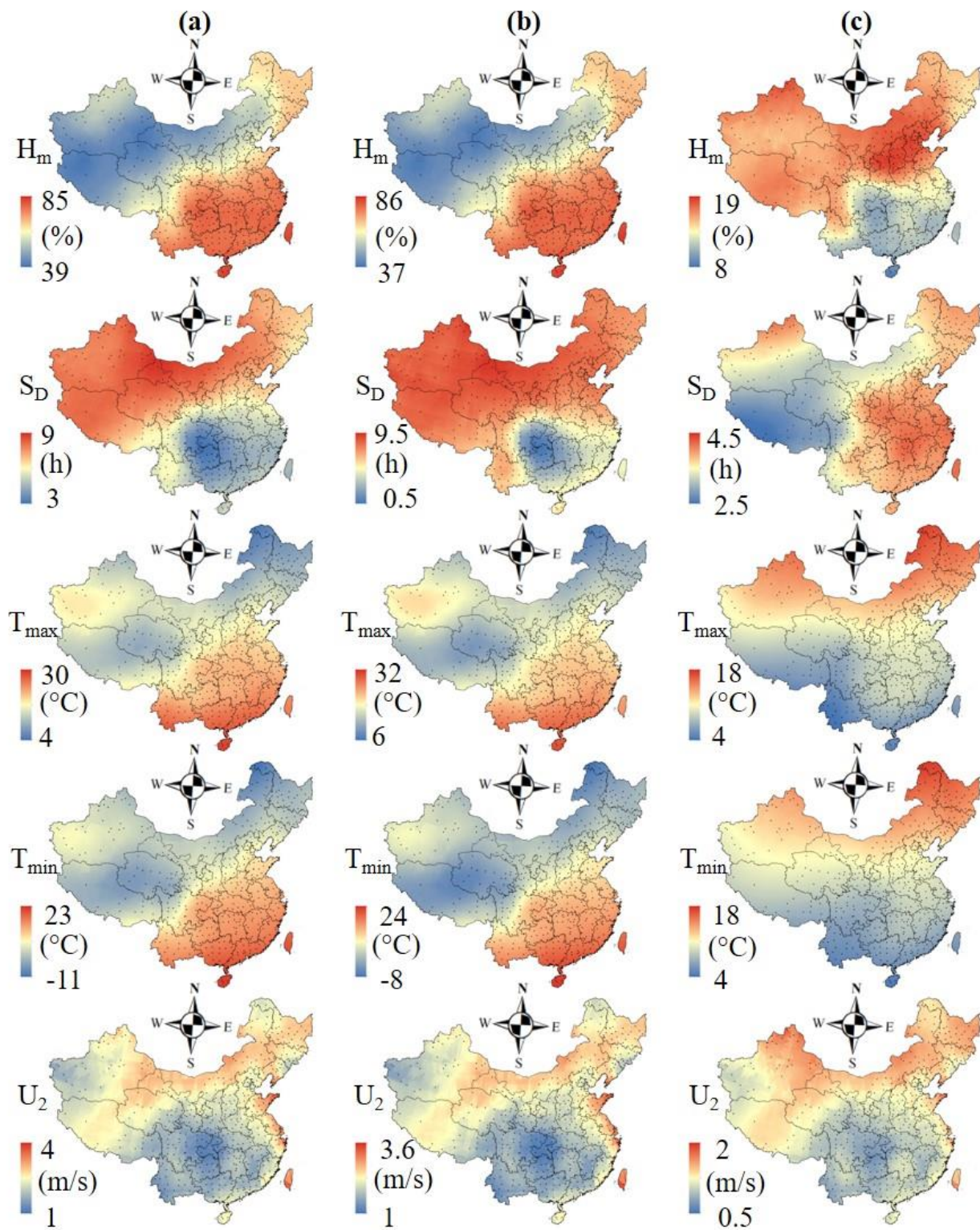


Figure 4. Descriptive statistics of the daily climatic variables: (a) mean; (b) median; and (c) standard deviation.

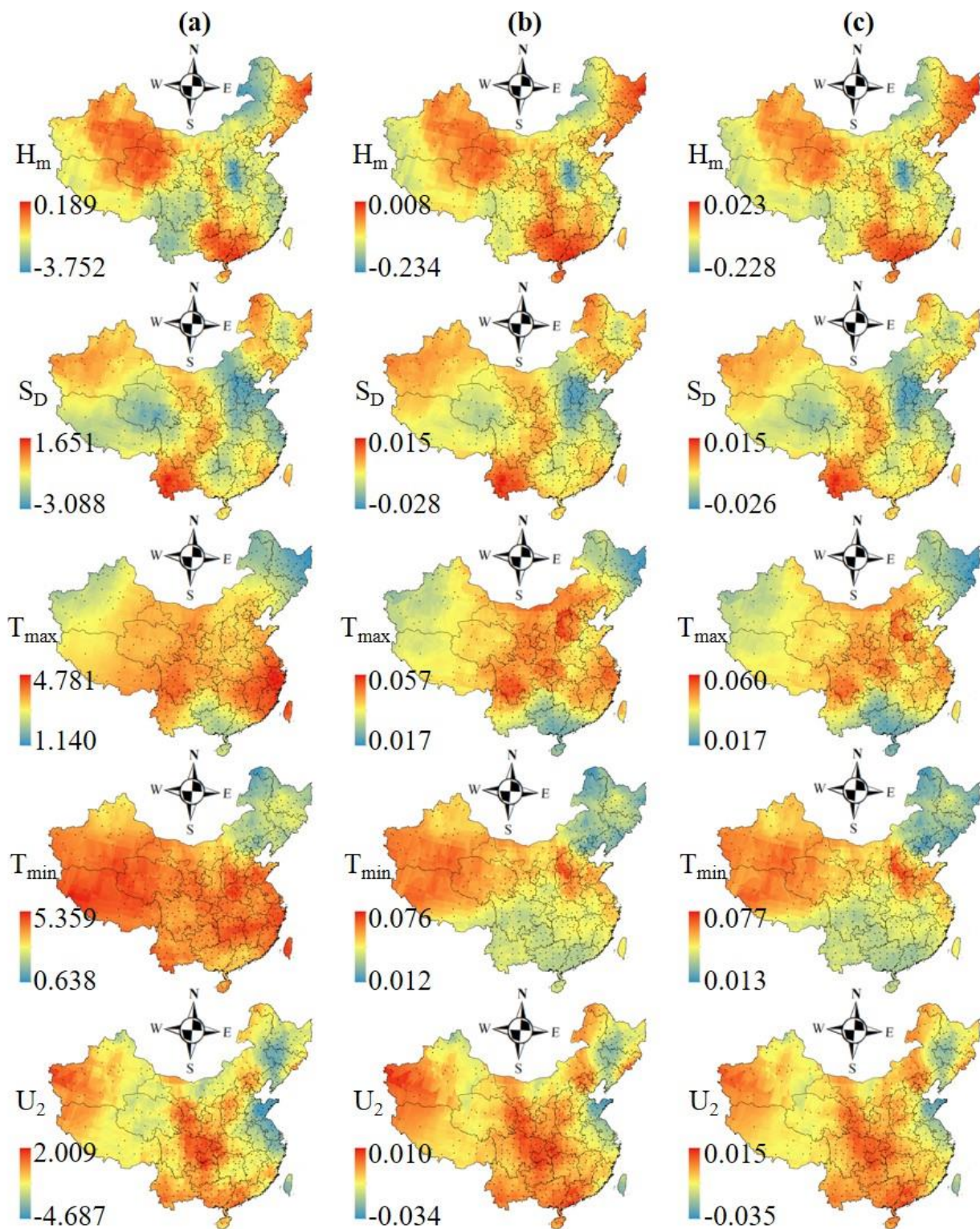


Figure 5. Spatial distribution maps for the trend analysis of the climatic variables: (a) M–K Z_s , (b) Sen’s slope, and (c) linear trend.

4. Discussion

4.1. Variability of ET_0 at Various Spatial Scales

The descriptive statistics of daily ET_0 for each station (at the local scale) have been presented in Figure 2 and the mean values were averaged to obtain the mean ET_0 at the provincial, regional, and continental scales. This averaging approach was used for upscal-

ing, instead of other approaches based on interpolations, to avoid the large uncertainties caused by spatial interpolations. At the continental scale, the daily ET_0 across China for 1984–2019 was 2.72 mm/day. However, the standard deviation of the mean daily ET_0 at different stations was 0.40 mm/day, which was quite high, indicating that the ET_0 characteristics found at the continental scale cannot provide meaningful insight for local water management. Wang et al. [26] investigated the spatiotemporal variability of ET_0 during 1961–2013 using a gridded dataset and also revealed that the ET_0 in China differed significantly. Thus, the ET_0 variation characteristics across different spatial scales should be investigated.

At the regional scale, the averaged daily ET_0 was the highest in South China (SCR), which was 3.25 mm/day, followed by NWR (2.80 mm/day), NCR (2.78 mm/day), ECR (2.76 mm/day), SWR (2.69 mm/day), and CCR (2.68 mm/day). The averaged ET_0 was the lowest in North East (NER), which was 2.24 mm/day.

Figure 6 illustrates the time series of annual mean daily ET_0 at the provincial scale. In the area NER, province LN generally had the highest ET_0 (mean ET_0 = 2.51 mm/d), while HL had the lowest ET_0 (mean ET_0 = 2.06 mm/d). Province TJ had the highest ET_0 (mean ET_0 = 3.01 mm/d) in the subregion NCR, and NM had the lowest ET_0 (mean ET_0 = 2.61 mm/d). In ECR, the ET_0 was the highest in province SH (mean ET_0 = 2.83 mm/d) and the lowest in AH (mean ET_0 = 2.60 mm/d). In the subregion SCR, ET_0 ranged from 2.96 mm/d in GX to 3.60 mm/d in HI. In the subregion CCR, the difference in ET_0 was relatively small, with HA being the province with the highest ET_0 (mean ET_0 = 2.80 mm/d) and HB being the province with the lowest ET_0 (mean ET_0 = 2.61 mm/d). The province that had the maximum mean ET_0 in the subregion NWR was XJ (mean ET_0 = 3.06 mm/d), and the one that had the minimum mean ET_0 was QH. In the subregion SWR, the mean ET_0 ranged from 2.47 mm/d in province CQ to 3.02 mm/d in YN. In some areas, such as SCR, the differences at different locations were relatively small, and thus, it is reasonable to estimate ET_0 characteristics at a smaller spatial scale using ET_0 characteristics at a larger spatial scale. However, most of the regions exhibited significant differences of ET_0 at different locations; thus, the regional observations cannot well represent the provincial characteristics.

The trends in ET_0 variations at the local scale have been presented in Figure 3, and the trends at the provincial and regional scales can be analyzed based upon these trends. The statistics regarding the trends in ET_0 at the regional scale are summarized in Figure 7. In the subregion NCR, 34% of the stations showed a trend of “increase-significant $\alpha = 0.01$ ”, followed by “increase” (28%) and “increase-significant $\alpha = 0.05$ ” (18%). In the area ECR, 39% of the stations showed a trend of “increase”, followed by “decrease” (26%) and “increase-significant $\alpha = 0.01$ ” (20%). 39% of the stations in the subregion SCR showed a trend of “increase”, while 25% showed a trend of “decrease” and 22% showed a trend of “increase-significant $\alpha = 0.05$ ”. In the area SWR, a large portion of the stations showed a trend of “increase” (45%) and “increase-significant $\alpha = 0.01$ ” (31%), and 12% of the stations showed a trend of “decrease”. There were 39%, 27%, and 13% of the stations in the subregion NWR that showed a trend of “increase-significant $\alpha = 0.01$ ”, “increase”, and “decrease” (13%), respectively. The majority of the stations in CCR showed an increasing trend (34% “increase” and 30% “increase-significant $\alpha = 0.01$ ” (30%)), and there were also 26% that showed the “decrease” trend. In the subregion NER, most of the stations (44%) showed a trend of “increase”; however, there were also 26% of the stations showed a trend of “decrease” (26%), exhibiting a significant diverse; the portion of stations that showed a trend of “increase-significant $\alpha = 0.01$ ” was 16%. At the continental scale, the annual ET_0 increased by approximately 12 mm/decade for 1984–2019. Most of the stations showed increasing trends, with 36% of the stations exhibiting a trend of “increase” and 27% exhibiting “increase-significant $\alpha = 0.01$ ” (27%); however, there were also 19% of the stations that showed a trend of “decrease”. Zhang et al. [31] studied evapotranspiration (ET) in China for 1948–2018 and found that the ET in most regions (covered by 89.5% pixels) showed increasing trends, which was close to the current observation. Zhang et al. [31] reported that the fluctuation of ET was relatively larger in the north and west, and relatively weaker in the south and east.

The present study found the same characteristic, but it reported the standard deviations and variances of ET_0 variations at each station to quantitatively describe the fluctuations (Figure 2).

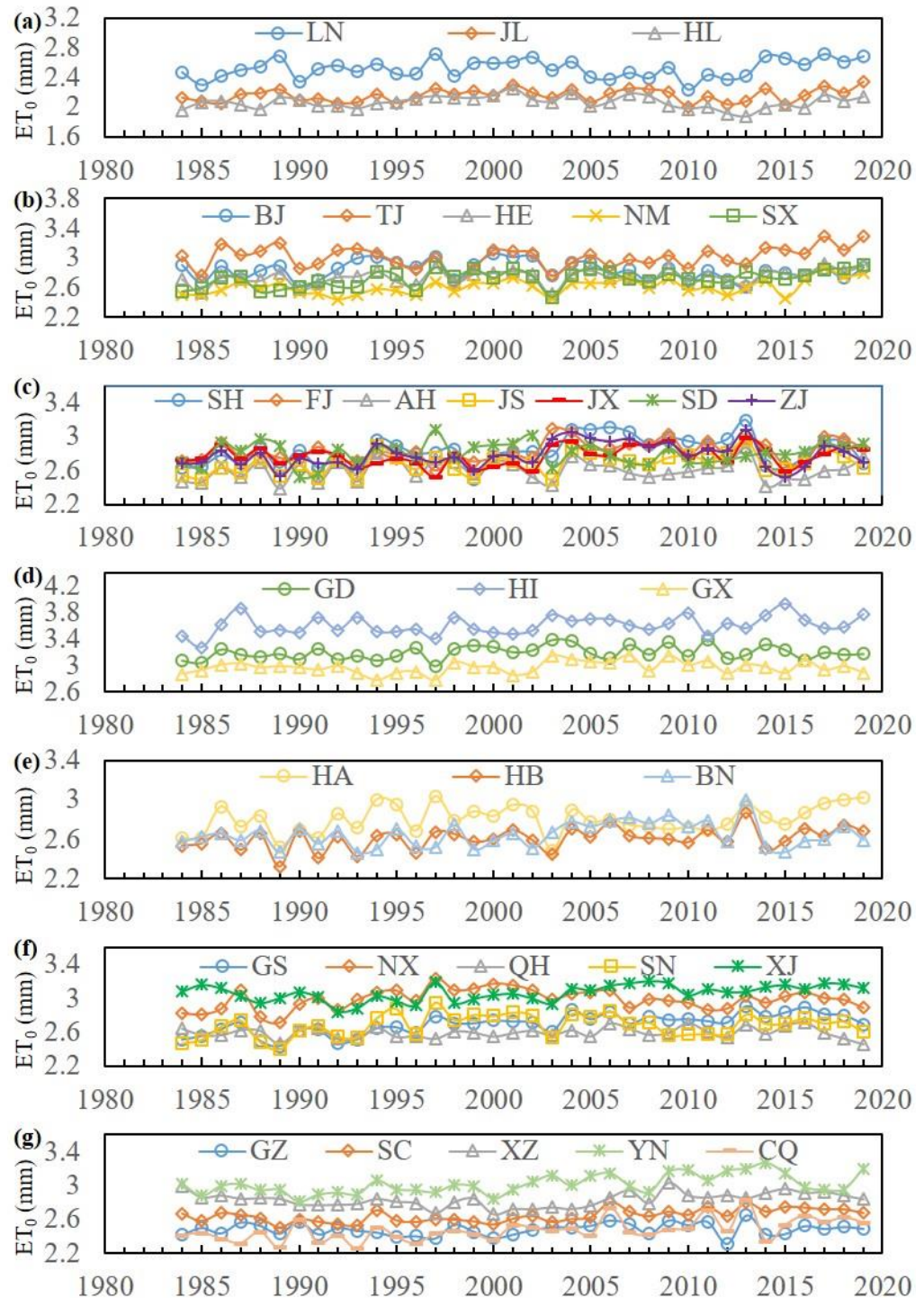


Figure 6. Annual mean daily ET_0 in different regions: (a) NE; (b) NCR; (c) ECR; (d) SCR; (e) CCR; (f) NWR; (g) SWR.

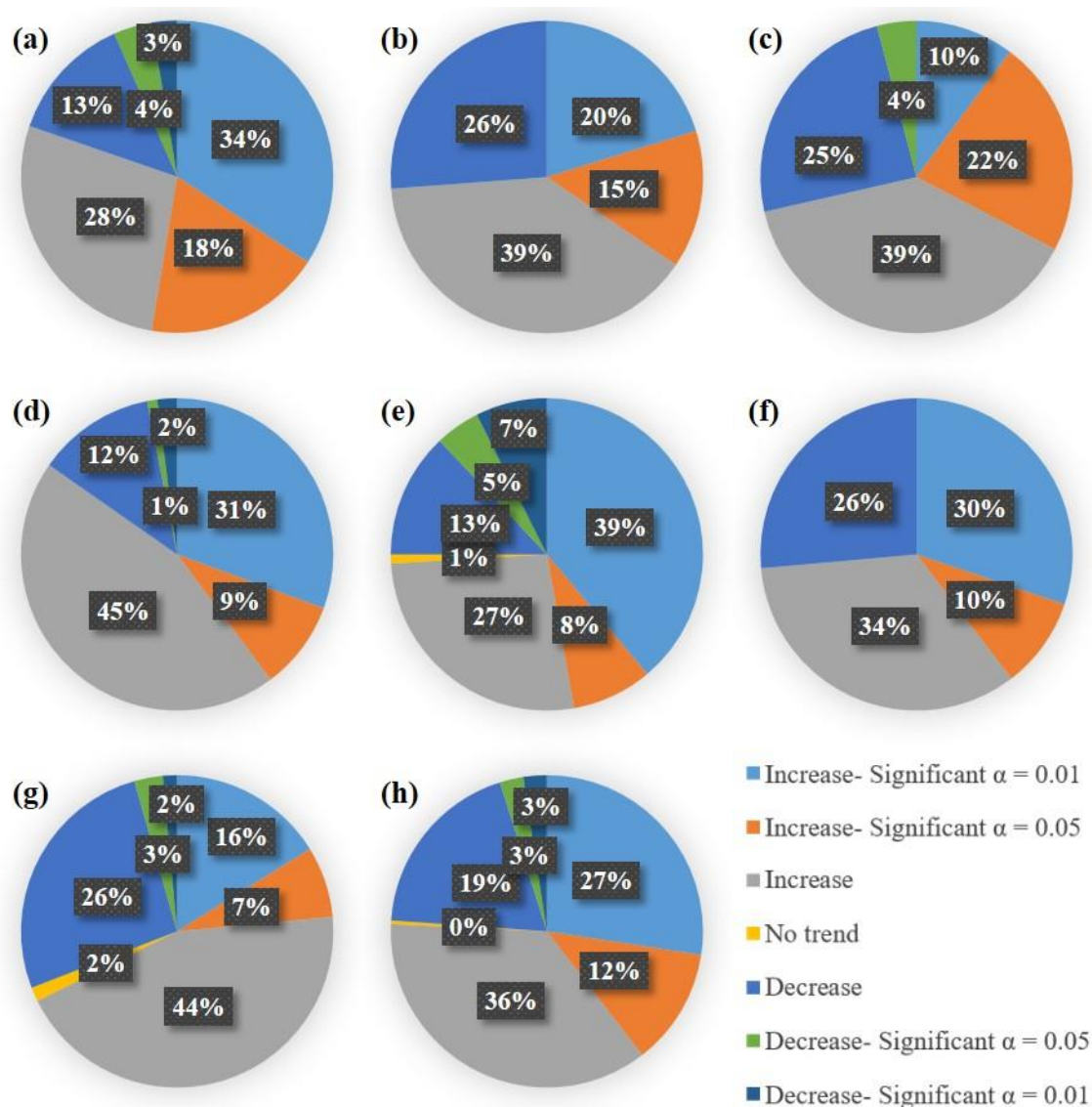


Figure 7. Statistics of the trend levels in different regions: (a) NCR; (b) ECR; (c) SCR; (d) SWR; (e) NWR; (f) CCR; (g) NER; and (h) National.

4.2. Variability of Climatic Variables at Various Spatial Scales

The statistics at the regional and continental (national) scales are illustrated in Figure 8, in which the trends and M-K Z_s values are also indicated. The lower lines of the boxes indicated the lower quartiles, which were the medians of the lower half of the datasets, the medium lines correspond to the middle values of the entire datasets, and the upper lines indicate the upper quartiles, which were the medians of the upper half of the datasets. These lines of boxes can also provide insight for the variability of climatic variables at the provincial scale.

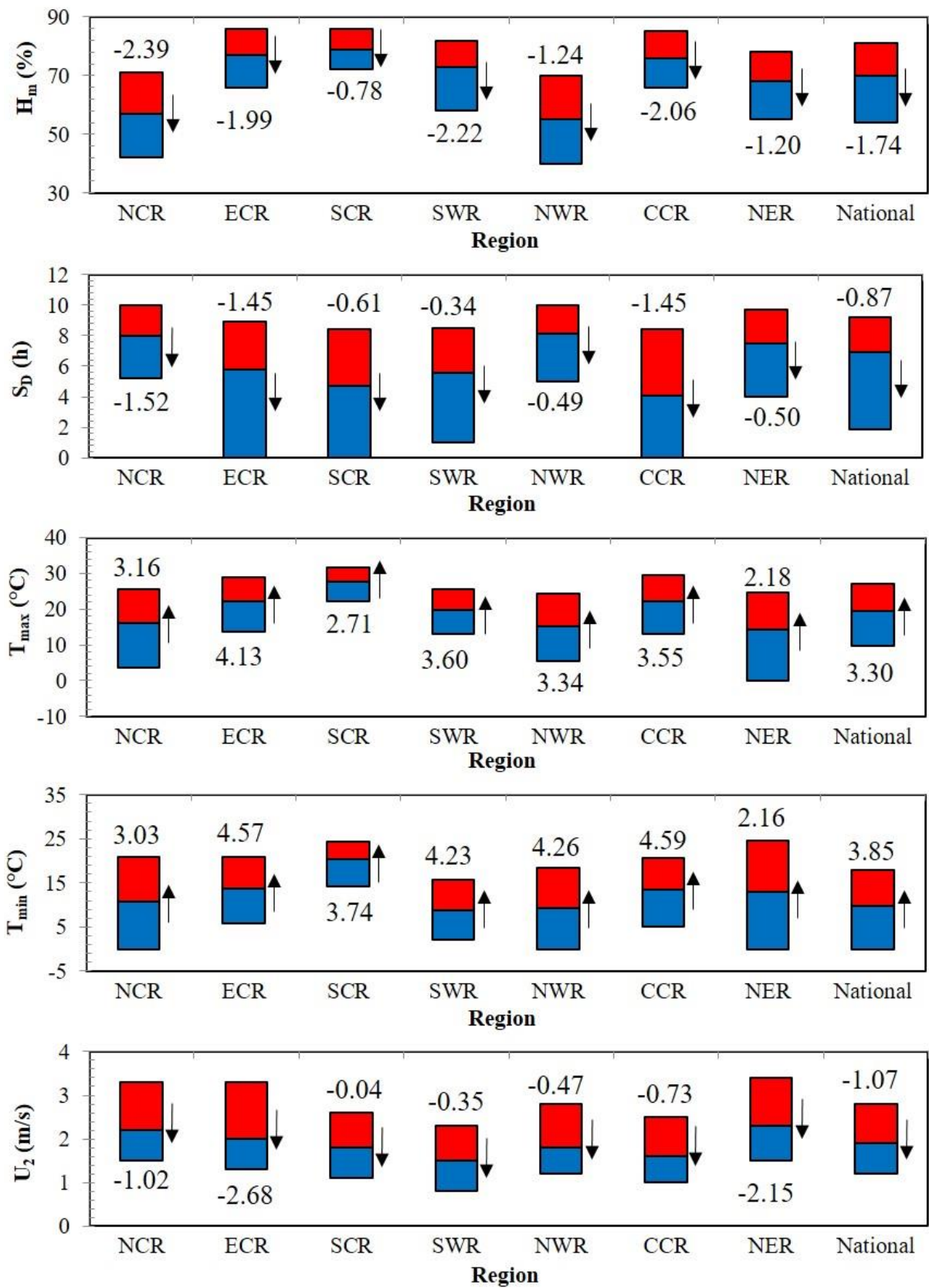


Figure 8. Statistics of the climatic factors in different subregions. The lower line = the lower quartile; the medium line = the middle values; the upper line = the upper quartile; the arrow = the trend; and the numbers = the values of Z_s .

As can be seen, the H_m in ECR, SCR, and CCR was relatively higher, whereas that in NCR and NWR was relatively lower. All of the subregions showed decreasing trends in H_m , with NCR having the most significant trend ($Z_s = -2.39$) and SCR having the least significant trend rate ($Z_s = -0.78$). The subregions NCR, NWR, and NER had relatively greater values of S_D than the other subregions. S_D was declining in all of the areas, and the absolute value of Z_s was the largest in NCR ($Z_s = -1.52$) and smallest in SWR ($Z_s = -0.34$). Yin et al. [15] has studied the potential evapotranspiration (PET) and its determining factors in China for 1971–2008 and has also found a decreasing trend of SD. T_{max} in SCR, CCR, and ECR was relatively higher than others in NCR and NER. All of the areas showed increasing trends, with the Z_s values ranging from 2.18 in NER to 4.13 in ECR. Similarly, T_{min} was also increasing in all of the subregions. T_{min} in ECR, SCR, and NER was relatively higher, whereas that in NCR and NWR was relatively lower. The Z_s values for T_{min} ranged from 2.16 in NER to 4.59 in CCR. In contrast to T_{max} and T_{min} , U_2 showed a decreasing trend, with SCR having the most significant trend rate ($Z_s = -0.04$) and ECR having the least significant ($Z_s = -2.68$). The subregions with relatively high U_2 included NCR, ECR, and NER, and those subregions with low U_2 included SWR, SCR, and CCR. Yin et al. [15] has also found that U_2 showed a decreasing trend. In summary, the results at the continental scale can well represent the trend directions at the regional scale. In some regions, the findings at the regional scale can satisfactorily represent the characteristics at the provincial and local scales, such as H_m in SCR and T_{max} in SWR. However, in most regions, both the statistics and trend rates exhibited substantial variations across spatial scales, such as S_D in ECR and T_{min} in NER.

4.3. Sensitivity and Contribution

The variations in ET_0 are the combined effects of the climatic variables; thus, it is important to quantify the sensitivity of ET_0 to these factors for a better understanding of the driving mechanisms. The mean values of the sensitivity coefficients, the corresponding trends (Z_s values), and trend rates (Sen's slope) at the local scale are presented in Figure 9.

Figure 9 shows that ET_0 at most stations was negatively correlated to the variations in H_m , while ET_0 at most stations was positively correlated to the variations in the other climatic variables. At the continental scale, ET_0 was most sensitive to H_m (average $S_t = -0.66$), followed by T_{max} ($S_t = 0.29$), S_D ($S_t = 0.18$), U_2 ($S_t = 0.16$), and T_{min} ($S_t = 0.07$). Yin et al. (2010) also revealed that H_m was the most sensitive variable for PET.

Consistent with the observations of Fan and Thomas [29], who studied ET_0 in China for the period of 1960–2011, the importance of the climatic variables to ET_0 were not stable. Most of the stations showed increasing trends in S_t for H_m (56.16%), with a Z_s value of 0.37 and a slope of 0.00092 at the continental scale. Fan and Thomas [29] has also found that the importance of H_m increased in China. In terms of S_D , 69.78% of the stations showed decreasing trends, and the Z_s value and slope at the continental scale were -1.15 and -0.00027 , respectively. Liu et al. [25] found that the sensitivity of T_{max} exhibited declining trends while that of T_{min} showed increasing trends in China for 1960–2007. However, based on the present study, which covered a longer time period, the majority of the stations showed increasing trends in S_t for T_{max} (72.95%) and T_{min} (87.31). The Z_s values at the continental scale corresponding to T_{max} and T_{min} were 1.25 and 2.16, respectively, and the slopes at the continental scale were 0.00040 and 0.00032, respectively. Interestingly, 90.49% of the stations showed increasing trends in S_t for U_2 , implying that U_2 was becoming more important in affecting ET_0 . Liu et al. [25] also found that the sensitivity of U_2 showed an increasing trend in China for 1960–2007. The Z_s value and slope at the continental scale corresponding to U_2 was 2.38 and 0.00106, respectively.

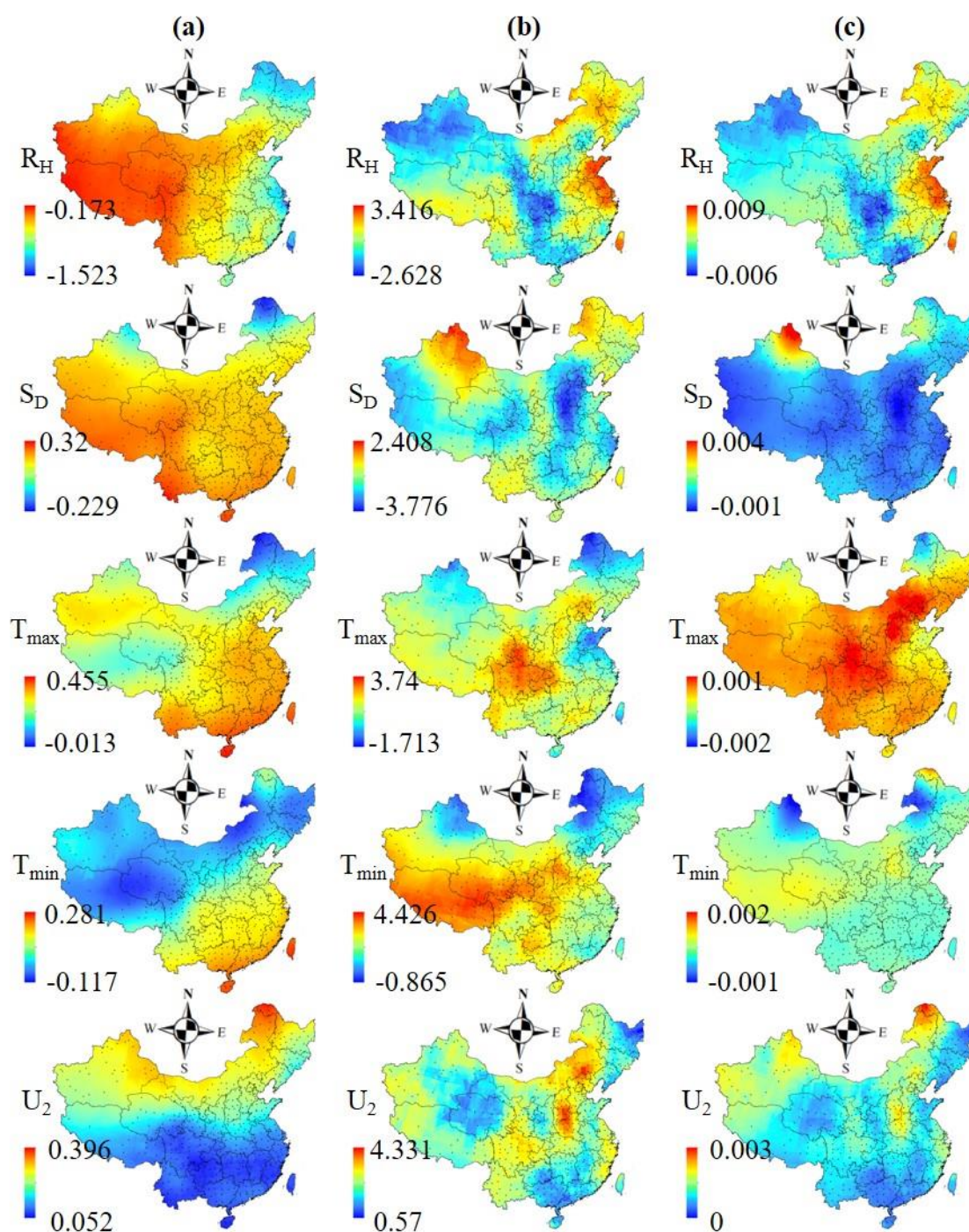


Figure 9. Sensitivity coefficients for the climatic factors: (a) mean; (b) M-K Z_s ; and (c) Sen's slope.

The contribution of each climatic variable to the variation in ET_0 was quantified in Figure 10, in which the spatial distribution of Z_s for ET_0 was also shown for a better interpretation of the climatic effects. As can be seen from Figure 10, the variations in H_m increased ET_0 at most of the stations (441 stations; 82.28%), and the C_b at the continental scale was 2.83%. Similarly, the variations in T_{max} and T_{min} increase ET_0 at 526 stations (98.13%) and 370 stations (69.03%), respectively, and the C_b values at the continental scale were 2.32% and 0.07%, respectively. However, for most stations, the variations in S_D and U_2 decreased ET_0 at most of the stations (354 stations and 302 stations, respectively), and the C_b values at the continental scale were -0.67% and -0.70% , respectively. Yao et al. [30] studied the PET across China for 1982–2010 and found that PET was mostly attributed

to the incident solar radiation, followed by pressure deficit, air temperature, and wind speed, which were close to the current observations. Ullah et al. [40] and Hina et al. [41] investigated the climatic variables related to drought and possible cycles over Pakistan. The analysis of atmospheric circulation patterns revealed that large-scale changes in wind speed, air temperature, relative humidity, and so on are the likely drivers of droughts in the region, which also confirmed the current observations were reasonable. Sein et al. [42] assessed the spatiotemporal variation of summer monsoon precipitation and its potential drivers in Myanmar and found that the spatial trends for monthly and seasonal precipitation vary from station to station and region to region due to a fluctuated shift of climatic dynamics, which demonstrated the precipitation and ET_0 variability is associated with regional scale atmospheric circulation and some climatic variables. Based on the values of C_b obtained in this study using the latest dataset, it can be concluded that the variations in ET_0 were mostly attributed to H_m , T_{max} , U_2 , S_D , and T_{min} .

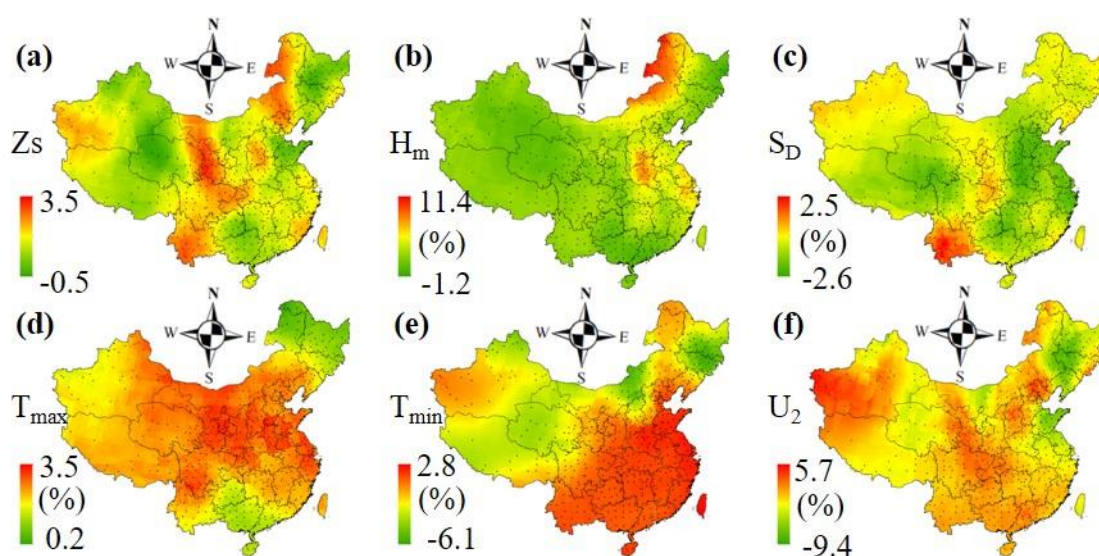


Figure 10. Spatial maps for the contribution analysis: (a) the M–K Z_s value of ET_0 ; (b) the C_b of RH; (c) the C_b of S_D ; (d) the C_b of T_{max} ; (e) the C_b of T_{min} ; and (f) the C_b of U_2 .

5. Conclusions

Daily ET_0 at 536 meteorological stations in China for the period 1984–2019 were calculated, the trends in ET_0 and its contributing climatic variables were analyzed, and the sensitivity of ET_0 to the meteorological variables and the contribution rates of the meteorological variables to the ET_0 variations were discussed. A key novelty of this study was that the variability of ET_0 and the contributing meteorological variables at various spatial scales were investigated. Generally, ET_0 decreased from south to north. The core of high ET_0 was primarily located near the southern edge. Generally, the standard deviation and variance decreased from north to south, and the kurtosis and skewness increased from northeast to southwest. The ET_0 increased at 406 of the 536 stations, and the averaged slope showed that the annual ET_0 increased by approximately 12 mm/decade in China. Most of the stations showed decreasing trends in H_m ($Z_s = -1.74$), S_D ($Z_s = -0.87$), and U_2 ($Z_s = -1.07$) and increasing trends in T_{max} ($Z_s = 3.30$) and T_{min} ($Z_s = 3.85$).

ET_0 was negatively correlated to H_m , and the average sensitivity coefficient was -0.66 . In terms of positively correlated variables, ET_0 was most sensitive to T_{max} ($S_t = 0.29$), followed by S_D ($S_t = 0.18$), U_2 ($S_t = 0.16$), and T_{min} ($S_t = 0.07$). The S_t for H_m at most stations (56.16%) were increasing while the S_D at most stations (69.78%) were decreasing. The majority of the stations showed increasing trends in S_t for T_{max} (72.95%) and T_{min} (87.31%). Interestingly, 90.49% of the stations showed increasing trends in S_t for U_2 , implying that U_2 was becoming more important in affecting ET_0 . The variations in H_m , T_{max} , and T_{min} increased the ET_0 at most of the stations (the mean contribution rate was 2.83%, 2.32%, and

0.07%, respectively). However, at most stations, the variations in S_D and U_2 decreased ET_0 , and the mean C_b values were -0.67% and -0.70% , respectively.

The present study reported an analysis of trends in ET_0 and its contributing climatic variables at four different spatial scales. Compared to analyses of a single or two spatial scales, the present analysis can better illustrate the variation trends and aid in future studies in water resources, agriculture, and hydrology in China. This study is also meaningful for modeling of hydrodynamics and water quality in inland and coastal water: first, the data can be directly used as inputs of the models; and second, the studied ET_0 characteristics can provide a better understanding of the mechanics and reasons for the variations in hydrodynamics and water quality. The present study found that the variations in ET_0 , climatic variables, sensitivity coefficients, and contribution rates were significant at some stations, so it is important to regularly update the corresponding forecasts. The significant variations also emphasize that it is important to develop sustainable water resources management and water-saving irrigation techniques under the condition of climate change. This study used the averaging approach for upscaling, it deserves a separate study to perform other upscaling techniques to study ET_0 characteristics at different scales.

Author Contributions: Funding acquisition, methodology, project administration, writing original draft, X.Y.; Funding acquisition, investigation, writing review and editing, A.M.; Methodology, visualization, R.A.; Writing review and editing, J.L.; Writing review and editing, X.C. All authors have read and agreed to the published version of the manuscript.

Funding: This research was funded by the Fundamental Research Funds for the Central Universities (China; DUT20RC(3)096), and Natural Sciences and Engineering Research Council of Canada (NSERC Discovery Grants).

Institutional Review Board Statement: Not applicable.

Informed Consent Statement: Not applicable.

Data Availability Statement: The data supporting reported results can be found from the China Meteorological Administration (<http://data.cma.cn> (accessed on 10 August 2022)).

Acknowledgments: The research is supported by the Fundamental Research Funds for the Central Universities (China; DUT20RC(3)096). We would like to thank the China Meteorological Administration for providing the daily meteorological data.

Conflicts of Interest: The authors declare no conflict of interest.

List of Acronyms and Symbols

ET_0	reference evapotranspiration;
H_m	humidity;
S_D	sunshine duration;
T_{max}	maximum air temperature;
T_{min}	minimum air temperature;
U_w	wind speed;
U_2	U_w at 2 m height;
U_{10}	U_w at 10 m height;

References

1. Luo, Y.; Chang, X.; Peng, S.; Khan, S.; Wang, W.; Zheng, Q.; Cai, X. Short-term forecasting of daily reference evapotranspiration using the Hargreaves–Samani model and temperature forecasts. *Agric. Water Manag.* **2014**, *136*, 42–51. [[CrossRef](#)]
2. Luo, Y.; Traore, S.; Lyu, X.; Wang, W.; Wang, Y.; Xie, Y.; Jiao, X.; Fipps, G. Medium Range Daily Reference Evapotranspiration Forecasting by Using ANN and Public Weather Forecasts. *Water Resour. Manag.* **2015**, *29*, 3863–3876. [[CrossRef](#)]
3. Aouissi, J.; Benabdallah, S.; Chabaâne, Z.L.; Cudennec, C. Evaluation of potential evapotranspiration assessment methods for hydrological modelling with SWAT—Application in data-scarce rural Tunisia. *Agric. Water Manag.* **2016**, *174*, 39–51. [[CrossRef](#)]
4. Yang, Y.; Cui, Y.; Luo, Y.; Lyu, X.; Traore, S.; Khan, S.; Wang, W. Short-term forecasting of daily reference evapotranspiration using the Penman-Monteith model and public weather forecasts. *Agric. Water Manag.* **2016**, *177*, 329–339. [[CrossRef](#)]
5. Yang, Y.; Cui, Y.; Bai, K.; Luo, T.; Dai, J.; Wang, W.; Luo, Y. Short-term forecasting of daily reference evapotranspiration using the reduced-set Penman-Monteith model and public weather forecasts. *Agric. Water Manag.* **2019**, *211*, 70–80. [[CrossRef](#)]

6. Chen, Z.; Zhu, Z.; Jiang, H.; Sun, S. Estimating daily reference evapotranspiration based on limited meteorological data using deep learning and classical machine learning methods. *J. Hydrol.* **2020**, *591*, 125286. [[CrossRef](#)]
7. Yan, X.; Mohammadian, A. Forecasting daily reference evapotranspiration for Canada using the Penman–Monteith model and statistically downscaled global climate model projections. *Alex. Eng. J.* **2020**, *59*, 883–891. [[CrossRef](#)]
8. Yan, X.; Mohammadian, A. Estimating future daily pan evaporation for Qatar using the Hargreaves model and statistically downscaled global climate model projections under RCP climate change scenarios. *Arab. J. Geosci.* **2020**, *13*, 1–15. [[CrossRef](#)]
9. Yin, J.; Deng, Z.; Ines, A.V.; Wu, J.; Rasu, E. Forecast of short-term daily reference evapotranspiration under limited meteorological variables using a hybrid bi-directional long short-term memory model (Bi-LSTM). *Agric. Water Manag.* **2020**, *242*, 106386. [[CrossRef](#)]
10. Iyakaremye, V.; Zeng, G.; Yang, X.; Zhang, G.; Ullah, I.; Gahigi, A.; Vuguziga, F.; Asfaw, T.G.; Ayugi, B. Increased high-temperature extremes and associated population exposure in Africa by the mid-21st century. *Sci. Total Environ.* **2021**, *790*, 148162. [[CrossRef](#)] [[PubMed](#)]
11. Ullah, I.; Saleem, F.; Iyakaremye, V.; Yin, J.; Ma, X.; Syed, S.; Hina, S.; Asfaw, T.G.; Omer, A. Projected Changes in Socioeconomic Exposure to Heatwaves in South Asia Under Changing Climate. *Earth's Future* **2022**, *10*, e2021EF002240. [[CrossRef](#)]
12. Traore, S.; Luo, Y.; Fipps, G. Deployment of artificial neural network for short-term forecasting of evapotranspiration using public weather forecast restricted messages. *Agric. Water Manag.* **2016**, *163*, 363–379. [[CrossRef](#)]
13. Althoff, D.; Dias SH, B.; Filgueiras, R.; Rodrigues, L.N. ETo-Brazil: A Daily Gridded Reference Evapotranspiration Data Set for Brazil (2000–2018). *Water Resour. Res.* **2020**, *56*, e2020WR027562. [[CrossRef](#)]
14. Mohammadi, B.; Mehdizadeh, S. Modeling daily reference evapotranspiration via a novel approach based on support vector regression coupled with whale optimization algorithm. *Agric. Water Manag.* **2020**, *237*, 106145. [[CrossRef](#)]
15. Yin, Y.; Wu, S.; Dai, E. Determining factors in potential evapotranspiration changes over China in the period 1971–2008. *Chin. Sci. Bull.* **2010**, *55*, 3329–3337. [[CrossRef](#)]
16. Ahmadi, F.; Mehdizadeh, S.; Mohammadi, B.; Pham, Q.B.; Doan, T.N.C.; Vo, N.D. Application of an artificial intelligence technique enhanced with intelligent water drops for monthly reference evapotranspiration estimation. *Agric. Water Manag.* **2021**, *244*, 106622. [[CrossRef](#)]
17. Yan, S.; Wu, L.; Fan, J.; Zhang, F.; Zou, Y.; Wu, Y. A novel hybrid WOA-XGB model for estimating daily reference evapotranspiration using local and external meteorological data: Applications in arid and humid regions of China. *Agric. Water Manag.* **2021**, *244*, 106594. [[CrossRef](#)]
18. Tang, B.; Tong, L.; Kang, S.; Zhang, L. Impacts of climate variability on reference evapotranspiration over 58 years in the Haihe river basin of north China. *Agric. Water Manag.* **2011**, *98*, 1660–1670. [[CrossRef](#)]
19. Roy, D.K.; Barzegar, R.; Quilty, J.; Adamowski, J. Using ensembles of adaptive neuro-fuzzy inference system and optimization algorithms to predict reference evapotranspiration in subtropical climatic zones. *J. Hydrol.* **2020**, *591*, 125509. [[CrossRef](#)]
20. Lawrimore, J.H.; Peterson, T.C. Pan Evaporation Trends in Dry and Humid Regions of the United States. *J. Hydrometeorol.* **2000**, *1*, 543–546. [[CrossRef](#)]
21. Tebakari, T.; Yoshitani, J.; Suvanpimol, C. Time-Space Trend Analysis in Pan Evaporation over Kingdom of Thailand. *J. Hydrol. Eng.* **2005**, *10*, 205–215. [[CrossRef](#)]
22. Burn, D.H.; Hesch, N.M. Trends in evaporation for the Canadian Prairies. *J. Hydrol.* **2007**, *336*, 61–73. [[CrossRef](#)]
23. Cong, Z.T.; Yang, D.W.; Ni, G.H. Does evaporation paradox exist in China? *Hydrol. Earth Syst. Sci.* **2009**, *13*, 357–366. [[CrossRef](#)]
24. Liu, Q.; Mcvcar, R. Assessing climate change induced modification of penman potential evaporation and runoff sensitivity in a large water-limited basin. *J. Hydrol.* **2012**, *464–465*, 352–362. [[CrossRef](#)]
25. Liu, C.; Zhang, D.; Liu, X.; Zhao, C. Spatial and temporal change in the potential evapotranspiration sensitivity to meteorological factors in China (1960–2007). *J. Geogr. Sci.* **2012**, *22*, 3–14. [[CrossRef](#)]
26. Wang, Z.; Xie, P.; Lai, C.; Chen, X.; Wu, X.; Zeng, Z.; Li, J. Spatiotemporal variability of reference evapotranspiration and contributing climatic factors in China during 1961–2013. *J. Hydrol.* **2017**, *544*, 97–108. [[CrossRef](#)]
27. Jiang, S.; Liang, C.; Cui, N.; Zhao, L.; Du, T.; Hu, X.; Feng, Y.; Guan, J.; Feng, Y. Impacts of climatic variables on reference evapotranspiration during growing season in Southwest China. *Agric. Water Manag.* **2019**, *216*, 365–378. [[CrossRef](#)]
28. Fan, Z.-X.; Thomas, A. Spatiotemporal variability of reference evapotranspiration and its contributing climatic factors in Yunnan Province, SW China, 1961–2004. *Clim. Chang.* **2013**, *116*, 309–325. [[CrossRef](#)]
29. Fan, Z.-X.; Thomas, A. Decadal changes of reference crop evapotranspiration attribution: Spatial and temporal variability over China 1960–2011. *J. Hydrol.* **2018**, *560*, 461–470. [[CrossRef](#)]
30. Yao, Y.; Zhao, S.; Zhang, Y.; Jia, K.; Liu, M. Spatial and Decadal Variations in Potential Evapotranspiration of China Based on Reanalysis Datasets during 1982–2010. *Atmosphere* **2014**, *5*, 737–754. [[CrossRef](#)]
31. Zhang, F.; Geng, M.; Wu, Q.; Liang, Y. Study on the spatial-temporal variation in evapotranspiration in China from 1948 to 2018. *Sci. Rep.* **2020**, *10*, 1–13. [[CrossRef](#)] [[PubMed](#)]
32. Allen, R.G.; Pereira, L.S.; Raes, D.; Smith, M. *Crop Evapotranspiration—Guidelines for Computing Crop Water Requirements—FAO Irrigation and Drainage Paper 56*; FAO: Rome, Italy, 1998; Volume 300, p. D05109.
33. Blankenau, P.A.; Kilic, A.; Allen, R. An evaluation of gridded weather data sets for the purpose of estimating reference evapotranspiration in the United States. *Agric. Water Manag.* **2020**, *242*, 106376. [[CrossRef](#)]

34. Califano, F.; Mobilia, M.; Longobardi, A. Heavy Rainfall Temporal Characterization in the Peri-Urban Solofrana River Basin, Southern Italy. *Procedia Eng.* **2015**, *119*, 1129–1138. [[CrossRef](#)]
35. Mann, H.B. Nonparametric tests against trend. *Econom. J. Econom. Soc.* **1945**, *13*, 245–259. [[CrossRef](#)]
36. Kendall, M.G. *Rank Correlation Methods*, 4th ed.; Charles Griffin: London, UK, 1975.
37. Gocic, M.; Trajkovic, S. Analysis of changes in meteorological variables using Mann-Kendall and Sen's slope estimator statistical tests in Serbia. *Glob. Planet. Chang.* **2013**, *100*, 172–182. [[CrossRef](#)]
38. Ye, X.; Li, X.; Liu, J.; Xu, C.-Y.; Zhang, Q. Variation of reference evapotranspiration and its contributing climatic factors in the Poyang Lake catchment, China. *Hydrol. Process.* **2014**, *28*, 6151–6162. [[CrossRef](#)]
39. Sen, P.K. Estimates of the regression coefficient based on Kendall's tau. *J. Am. Stat. Assoc.* **1968**, *63*, 1379–1389. [[CrossRef](#)]
40. Ullah, I.; Ma, X.; Yin, J.; Saleem, F.; Syed, S.; Omer, A.; Habtemicheal, B.A.; Liu, M.; Arshad, M. Observed changes in seasonal drought characteristics and their possible potential drivers over Pakistan. *Int. J. Clim.* **2021**, *42*, 1576–1596. [[CrossRef](#)]
41. Hina, S.; Saleem, F.; Arshad, A.; Hina, A.; Ullah, I. Droughts over Pakistan: Possible cycles, precursors and associated mechanisms. *Geomat. Nat. Hazards Risk* **2021**, *12*, 1638–1668. [[CrossRef](#)]
42. Sein ZM, M.; Zhi, X.; Ullah, I.; Azam, K.; Ngoma, H.; Saleem, F.; Nkuzimana, A. Recent variability of sub-seasonal monsoon precipitation and its potential drivers in Myanmar using in-situ observation during 1981–2020. *Int. J. Climatol.* **2022**, *42*, 3341–3359. [[CrossRef](#)]